High-voltage pulse switching hardware for electro-optic studies of conducting aqueous solutions

Scott A. Riley, Skipp May, and Matthew P. Augustine[a)]
Department of Chemistry, One Shields Avenue, University of California, Davis, Davis, California 95616

(Received 27 December 2001; accepted for publication 22 April 2002)

The hardware necessary for the electro-optic study of conducting polyelectrolyte solutions is frequently not commercially available or financially practical. The designs of an electrical rectangular pulse switch and polarity-reversing relay switch capable of producing 3 kV 5 A direct current pulses lasting longer than 100 μs are presented. As an example of the operation of this equipment, the electric birefringence of an aqueous solution of the Pseudomonas bacteriophage Pf1 in *tris*/EDTA buffer is presented. © *2002 American Institute of Physics.*
[DOI: 10.1063/1.1489075]

I. INTRODUCTION

Electric birefringence and dichroism are valuable methods of determining the optical and electrical polarizability anisotropies, permanent electric dipole moments, and rotational diffusion constants of gas- and liquid-phase molecules.[1–4] These electro-optic measurements use a polarized light source to investigate molecular alignment induced by an external electric field E. In the absence of both an electric field and long-range intermolecular forces like those responsible for liquid-crystalline behavior,[5] molecules are randomly oriented and thus produce a medium that is optically isotropic. Upon application of an electric field molecules having a permanent electric dipole moment or anisotropic electric polarizability align, causing the bulk sample to become optically anisotropic. In the case of electric dichroism the difference in absorption of light parallel and perpendicular to the applied electric-field direction is measured ($\Delta A = A_{\parallel} - A_{\perp}$), whereas in electric birefringence the optical retardation δ is measured. The source of the phase shift δ is a difference in the velocity of light propagating through the medium mediated by index of refraction differences parallel and perpendicular to the applied electric-field direction ($\Delta n = n_{\parallel} - n_{\perp}$).[1]

The apparatus requirements for molecular electro-optic studies are sample dependent. For example, examination of aqueous-phase biological macromolecules like fragments of DNA,[4,6] the tobacco mosaic virus,[2,7,8] and bacteriophage[9] requires solutions of non-negligible ionic strengths with dc sample resistances less than 1000 Ω. In all of these studies, dc rather than ac electric fields are favored, presumably because larger alignment can be obtained for a given applied voltage and skin depth and Debye relaxation effects are circumvented. In an effort to minimize electrophoresis, electrolysis, and Joule heating in high-ionic-strength polyelectrolyte solutions, the dc electric field must be pulsed. Furthermore, for high-conductivity samples several amps of current are needed to sustain the $E > 10\,\mathrm{kV\,cm^{-1}}$ field required to saturate the molecular alignment. The duration of the applied electric-field pulse must be variable between 100 μs and several milliseconds and the polarity of the electric field across the sample should be alternated to further minimize electrophoresis and electrode polarization.

While many forms of apparatus have been discussed over the decades,[1–3,10–14] they are often not conducive to the study of biological samples in aqueous conducting solutions, not commercially available, and/or not financially practical. The aim of this article is to present the design of hardware that *is* applicable, available, and practical for biological electro-optic studies and to demonstrate the use of this equipment in the measurement of the electric birefringence of a Pseudomonas bacteriophage Pf1 solution.

II. EXPERIMENTAL SETUP

Figure 1 shows the schematic of the experimental setup used to measure electric birefringence. A Newport model 818 battery-biased *PIN* detector is used to convert the transient light signal generated by the induced birefringence to a voltage that is subsequently acquired with a 500 MHz maximum bandwidth Tektronix TDS 724C digitizing oscilloscope. Further analysis of the crude transients is performed offline using Matlab,[15] operating on a personal computer. A Spectra Physics model 164 continuous-wave Ar^+-ion laser tuned to a wavelength of $\lambda = 514$ nm is used as a light source with the maximum power always less than 5 mW. The Kerr cell consists of two polished stainless-steel 0.25 cm×1 cm×3 cm electrodes separated by 0.25 cm giving an $l = 3$ cm path length. The polarizer and analyzer are polarizing beam-splitting cubes set in a crossed configuration making an angle of 45° with respect to the direction of the applied electric field. This configuration allows determination of the magnitude of the optical retardation δ from the equation[1]

$$I = I_0 \sin^2(\delta/2), \tag{1}$$

where I_0 is the maximum light intensity measured by the detector when the polarizer and analyzer are parallel and I is the measured light intensity under the influence of the applied electric field with the optics crossed. The functional

a)Author to whom correspondence should be addressed; electronic mail: augustin@chem.ucdavis.edu

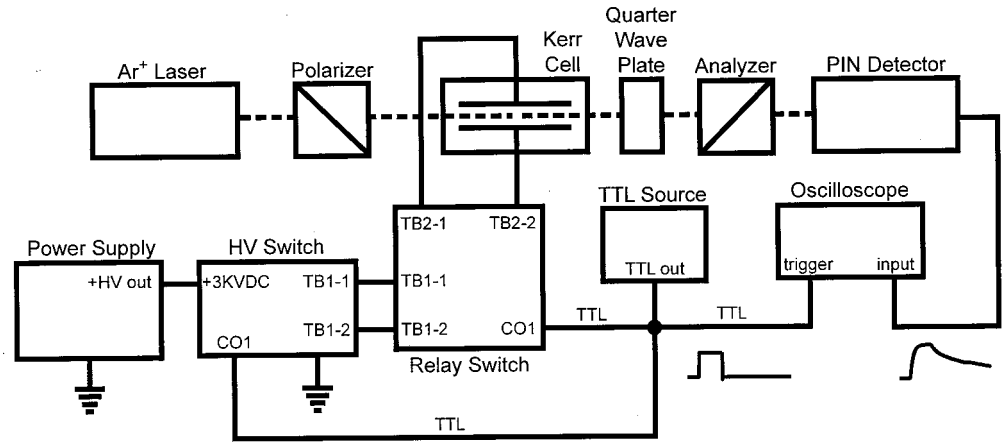

FIG. 1. Experimental setup for electric birefringence studies. The wiring connections for the rectangular pulse switch and polarity-reversing relay switch are included and correspond to the electrical schematics provided in Figs. 2 and 4.

form for the transmitted light in Eq. (1) implies that both positive and negative birefringence will produce an increase in light intensity at the detector. Rotation of the analyzer off the crossed position by an angle α and incorporation of a 514 nm quarter-wave plate between the sample and analyzer arranged with the fast axis parallel to the polarizer allows measurement of negative birefringence. In this way positive and negative birefringence correspond to a respective increase and decrease in light at the detector. This allows the determination of δ from the equation[1]

$$\Delta I = I - I_\alpha = I_0\{\sin^2(\alpha+\delta/2) - \sin^2\alpha\}, \tag{2}$$

where I and I_α are the intensities of light measured with and without an applied electric field when the analyzer is rotated off the crossed position by the angle α. The induced birefringence Δn in both cases can be calculated from the optical retardation as

$$\Delta n = \lambda\,\delta/2\pi l. \tag{3}$$

A TTL pulse from a Wavetek model 145 pulse/function generator is used to trigger data acquisition, gate the high-voltage rectangular pulse switch, and alternate the polarity-reversing relay switch as described in the hardware designs below. The high voltage is supplied by a homebuilt dc power supply capable of delivering 3.5 kV at 6 A in pulsed operation.[16]

Pseudomonas bacteriophage Pf1 is a 2-μm-long, 6-nm-diam electrically anisotropic semirigid particle that was prepared using the protocol described in Ref. 17. The phage was dialyzed repeatedly against 10 mM *tris*/EDTA buffer and diluted to the desired concentration, here 4.0 ± 0.2 μg mL^{-1}, as determined by ultraviolet visible spectroscopy using an extinction coefficient of $\epsilon_{270\,\mathrm{nm}} = 2.25\,\mathrm{mL\,mg^{-1}\,cm^{-1}}$. The buffer concentration following dilution was 10 μM.

III. DESIGN OF HARDWARE COMPONENTS

Reversible pulsed dc electric fields were established in conducting aqueous solutions using a rectangular pulse switch in combination with a polarity-reversing relay switch. The construction of this equipment from commercially available components is now described. As a word of caution, extreme care should be taken in the operation of this very high-voltage equipment.

A. Rectangular pulse switch

As already mentioned, the nature of electric birefringence experiments in aqueous solutions necessitates the use of a rectangular pulse switch. The need for versatility through TTL gating, reproducible high-voltage and current pulse outputs, and a voltage-scalable design, are all met by the use of metal–oxide field-effect-transistor (MOSFET) technology. It is well known that the avalanche MOSFETs introduced in the mid-1980s have successfully been used to switch or pulse complex loads. Advanced power technology (APT) (Ref. 18) manufactures several generations of power MOS *N*-channel enhancement mode power MOSFETs with exceptionally fast switching speeds and significantly lower on-state drain-to-source resistance loss, which can be easily applied to the construction of high-voltage and current rectangular pulse switches. A MOSFET switch design has the benefit of simplicity, low cost, and adjustable rise and fall times into complex (reactive) loads. Three or four generations of 1 kV rated BLL package *N*-channel APT power MOS devices were tested since the input capacitance C_{iss} between different device types and generations varies by as much as 1000 pF. The best performance was obtained with APT10090BLL ($C_{iss} = 2040$ pF) and APT10078BLL ($C_{iss} = 2510$ pF) devices.

Figure 2 shows a schematic of the rectangular pulse switch with an approximate parts cost of $400. Standard TTL control pulses are brought to the circuit via a coaxial cable CO1 that is terminated to prevent ringing. A low-value-disk ceramic capacitor C1 is paralleled to serve as a measure of radio-frequency (rf) noise suppression. An Allegro 6118a vacuum fluorescent display driver integrated circuit serves as a level shift and isolation buffer to provide an adjustable enhancement mode drive potential to the first APT MOSFET via a dip jumper block JP1. The jumper allows the signal load resistance path to the MOSFET to be easily opened for the evaluation of new 6118a devices. The low-current draw

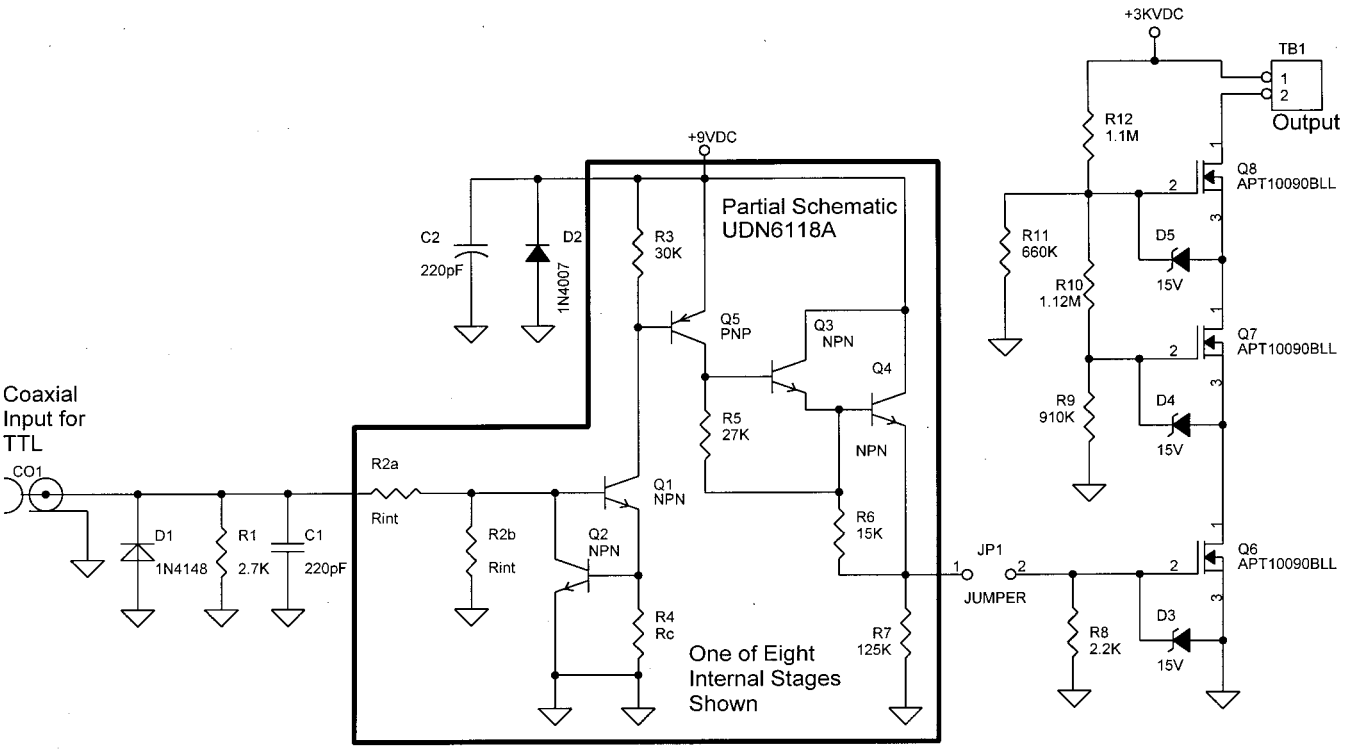

FIG. 2. Circuit diagram of the high-voltage rectangular pulse switch, which uses TTL-controlled high-power MOSFETs to produce 3 kV rectangular pulses with durations of 100 μs up to dc.

of the 6118a allows 9 V battery operation, which provides a measure of simplicity and safety. Reverse connection protection and noise filtering are provided by the adjacent discrete capacitors C2 and diodes D2, and the MOSFET gate termination resistance is provided by R8.

The high-voltage pulse switch section uses APT MOSFETs in a ''ladder'' device-stacking configuration—a geometry formerly accomplished with pulse-only units such as thyratron or *P*-channel-based devices. The first power MOSFET device Q6 functions as a straightforward 1 kV rated switch to ground. For a 3 kV switch, two additional MOSFETs Q7–Q8 are placed in series with the first in the previously mentioned ladder configuration. The typical data sheet drain–source on-state resistance of three APT10090BLL MOSFETs in series is listed as less than $R_{DS(on)}=3\ \Omega$. Zener diodes D3–D5 connecting the gate to source of each device ensure a safe maximum value of the gate-to-source turn-on voltage. The drain of MOSFET Q8 is connected through a terminal block TB1 to the ''grounding side'' of the potential-elevated Kerr cell through the polarity reversing relay switch described in the next section. True dc-to-ground pulses are generated in the Kerr cell by grounding one side of the cell through the pulse switch. A low-wattage virtuous-enameled resistor (not shown) in series with the cell is used as a fail-safe device to protect delicate biological samples. The value of this resistor, here 15 Ω at $\frac{1}{4}$ W, is chosen to act as a fuse and open the circuit if the switch fails and continuously drives the Kerr cell to ground. Low-duty-cycle pulsing with repetition rates of less than 50 Hz ensures that the resistor is not damaged in normal operation.

A voltage divider using resistors R9–R12 provides the applied Q7 and Q8 gate potentials, thereby establishing the operational range of each respective MOSFET in the ladder. Upon ''collapse'' of the lowest position MOSFET Q6, the adjacent device receives Zener-limited $V_{GS(th)}$ voltage, which permits rapid turn on. This action is repeated in the higher ladder MOSFETs until the entire ladder drain–source series is near ground potential. While the APT10090BLL MOSFET series provides excellent turn-on and turn-off delay times with a lower Miller gate charge and input capacitance, each generation of APT device requires minor drive potential adjustments. This is accomplished by initially constructing and testing the first stage of the switch consisting of only Q6. With the first stage functioning up to the 1 kV MOSFET rating, the second device Q7, along with voltage divider resistors R9 and R10, is added. Beginning with 2.2 MΩ high-voltage resistors, the values of R9–R10 are adjusted to optimize the wave-form rise and fall times, which may be monitored on an oscilloscope using a high-voltage probe to measure the drain potential of Q7. Addition of the third MOSFET Q8 and extension of the voltage divider network with R11 and R12 will require slight modification to the ratio of R9 and R10 to adjust the rise time. Resistors R11–R12 are then adjusted to achieve an optimal fall time. Through careful and custom selection of the R9–R12 values, the turn-on and turn-off times of the pulse switch can be adjusted to less than 20 μs.

Using a test resistance of 600 Ω at 25 W in place of a Kerr cell, the three-stage rectangular pulse switch performs well up to its maximum rated breakdown voltage of slightly higher than 3 kV, as seen in Fig. 3. Here, the 350 μs TTL pulse shown in Fig. 3(A) was used to gate the switch. The

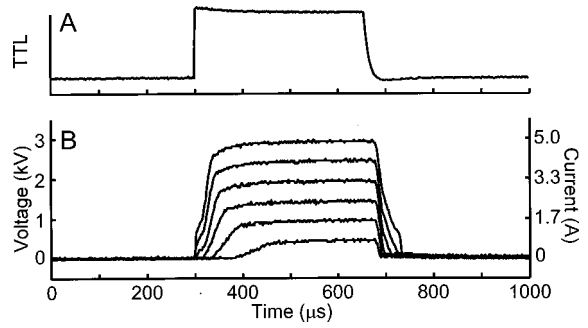

FIG. 3. Performance of the high-voltage rectangular pulse switch using 350 μs variable-amplitude pulses into a 600 Ω load. The pulse switch was gated using the TTL pulse shown in (A), resulting in the switch outputs shown in (B), where both voltage and current are displayed. Artifacts in the on and off times are due to the input capacitance of the MOSFET components and can be optimized by adjusting the voltage divider resistor network.

voltage across the 600 Ω load was digitized with an oscilloscope using a 1:1000 high-voltage probe, as shown in Fig. 3(B). The voltage transients show no current limiting in the dc power supply up to 3 kV with 5 A of current draw. It is clear that while full voltage is achieved during the pulse, there are voltage-dependent turn-on and turn-off delays due to the input capacitance of the MOSFETs. In order to insure TTL switch performance consistency and to provide crisp microsecond time-scale pulses at voltages less than 1 kV, Q7 and Q8 should be bypassed by connecting the second pin of the terminal block output TB1 to pin 1 of Q6 and disconnecting the voltage divider from the first pin of TB1. Operation of the switch above the 3 kV breakdown limit is possible with additional series devices and related voltage divider support circuitry.

B. Polarity-reversing relay switch

Figure 4 shows the schematic of the polarity-reversing relay switch with an approximate parts cost of $400. TTL-level switch commands are brought to the control board at CO1 and introduced to a common small signal transistor Q1 serving as buffer and logic inverter. This transistor also provides easy non-TTL-level interface capacity. As an example, a simple SPST switch may be added for manual operation.

The rising edge of the inverted positive control logic pulse from Q1 triggers a common dip package 555 timer U1 configured as a positive-edge clocked retriggered monostable timer. The 555 timer is configured to output a short control pulse whose length is determined by the adjacent resistor R3 and capacitor C1 values and is independent of the TTL-level switch duration. This output pulse is used to clock U2A—the first section of a common 4013 dual dip package CMOS flip-flop configured as a common binary divider with memory. The alternating-logic output of U2A provides the data input of U2B—the second section of the 4013 configured as a D-clock flip-flop. The Q-not output of U2B drives a common enhancement mode *N*-channel MOSFET Q2 that provides ground start on logic for two high-voltage high-speed SPDT vacuum relays LS1 and LS2. The coil of each relay is supplied with 26 V_{dc} through VCC with coil returns routed to the drain of Q2. A clamping diode D3 is placed from VCC to the drain lead junction in order to snub back emf from the relay coils.

The high-voltage relay connections are shown in the circuit diagram. Cross-connected poles with proper input and output connections provide polarity reversal of the applied high-voltage dc potential coming from the rectangular pulse switch through TB1. All connections are made with 40 kV

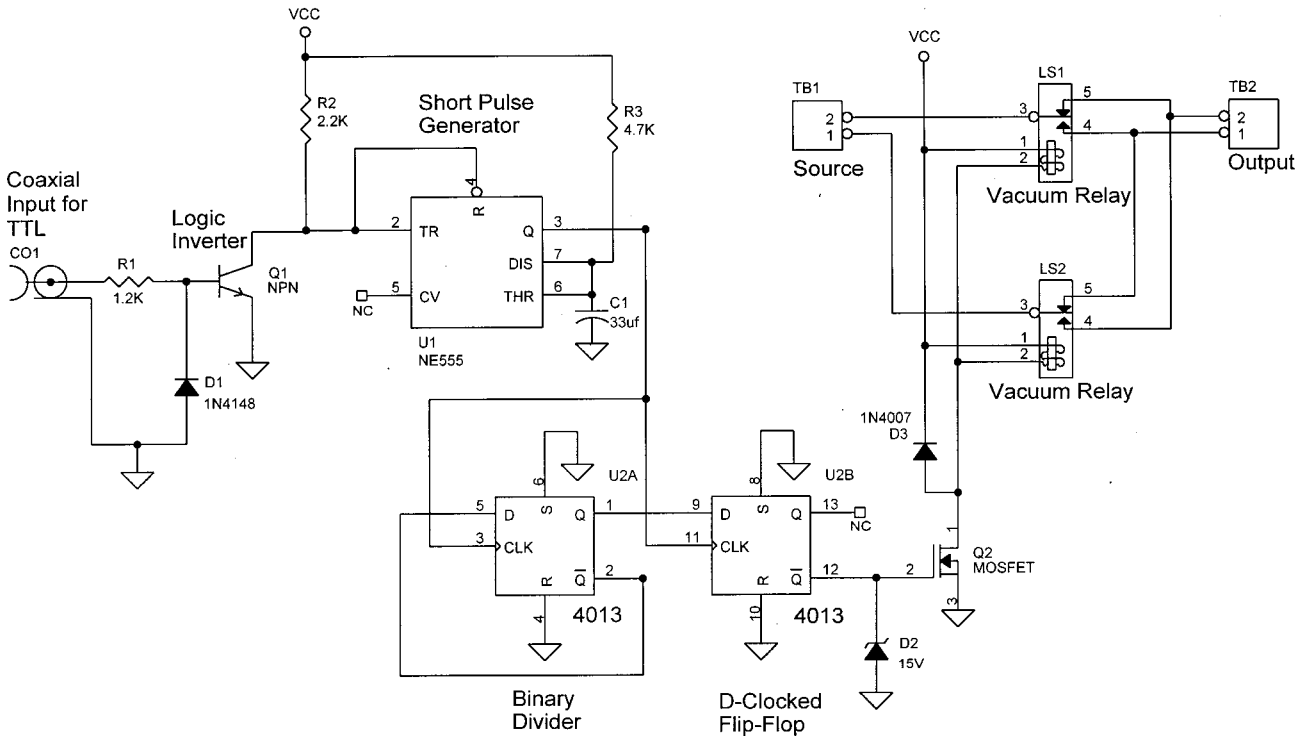

FIG. 4. Circuit diagram of the TTL-controlled polarity-reversing relay switch.

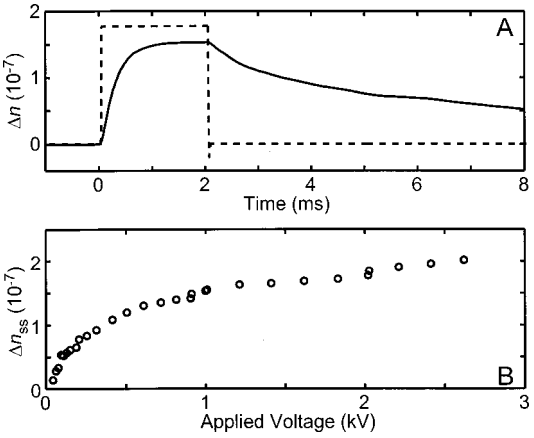

FIG. 5. Electric birefringence of a 4 $\mu g\,mL^{-1}$ Pf1 bacteriophage solution with 10 μM *tris*/EDTA buffer. The solid line in (A) shows the birefringence transient due to application of a 1 kV 2 ms pulse where the timing is shown as the dashed line. The steady-state birefringence shown in (B) is a function of the electric-field amplitude. Pulse lengths were varied from 6 to 0.5 ms for low-to-high potentials, respectively. The infinite field saturated birefringence was obtained from the data in (B) to be $\Delta n_{sat}=(2.46\pm0.03)\times10^{-7}$. Errors in the intensity of the steady-state birefringence are conservatively estimated by the size of the circles in (B).

rated wiring and each relay was mounted on Poly-plastic, Teflon, or Delrin-type insulating material. A common three-terminal regulator (not shown) through a simple voltage dropping resistor supplies voltage to the 555 and related support components. Connection to the Kerr cell is done through TB2.

IV. RESULTS AND DISCUSSION

The transient electric birefringence of the Pf1 solution was measured for several pulse amplitudes using the quarter-wave plate optics configuration described above with $\alpha=4°$. For voltages less than 1 kV only the first MOSFET stage of the rectangular pulse switch was used. All stages were employed for measurements of 1 kV or more. The polarity across the Kerr cell was reversed following each pulse to minimize electrode polarization and electrophoresis.

The solid line in Fig. 5(A) shows the birefringence transient corresponding to the 1 kV 2 ms pulse shown as the dashed line. All transients observed for this sample are positive, suggesting that the solution is dilute enough to avoid aggregation and intermolecular interaction effects. Upon application of the electric field, the phage begin to align parallel to the field[19] causing the sample to become birefringent. The birefringence increases until a steady-state alignment is reached at the end of the electric-field pulse. Upon removal of the electric field, alignment of the phage relaxes due to rotational diffusion until the solution is again isotropic. The pulse length is manually shortened as the voltage is raised to minimize electrolysis, and the steady-state birefringence Δn_{ss} is obtained from a fit of the measured transient to a rising exponential function.[8] The plot of Δn_{ss} versus applied voltage shown in Fig. 5(B) demonstrates that as the voltage across the sample, and thus the electric field in the sample, is increased the steady-state birefringence also increases until eventually all of the phage particles in the solution align. The alignment is thus saturated, resulting in a saturated birefringence Δn_{sat}, which can be determined experimentally by extrapolating the plot of Δn_{ss} versus voltage to an infinite electric field, where $\Delta n_{sat}=(2.46\pm0.03)\times10^{-7}$. By calculating Δn_{sat} relative to the solution concentration c as $\Delta n_{sat}/c=6.1_5\times10^{-5}\,mg^{-1}\,mL$, excellent agreement is found with birefringence measurements of Pf1 in high-magnetic fields, where $\Delta n_{sat}/c$ is $6.27\times10^{-5}\,mg^{-1}\,mL$.[20] In fact, an exact agreement between electrical and magnetic $\Delta n_{sat}/c$ values is achieved by simply assuming the concentration of Pf1 to be 3.92 $\mu g\,mL^{-1}$, a value well within the uncertainty of the spectroscopic determination of the 4.0 ± 0.2 $\mu g\,mL^{-1}$ concentration used here.

ACKNOWLEDGMENTS

Support from the NSF under Grant No. CHE-9504655 is gratefully acknowledged. One of the authors (M.P.A.) is a David and Lucile Packard Foundation and Alfred P. Sloan Foundation fellow.

[1] E. Fredericq and C. Houssier, *Electric Dichroism and Electric Birefringence* (Clarendon, Oxford, 1973).
[2] C. T. O'Konski, in *Electro-optics Series*, edited by Herbert Elion (Marcel Dekker, New York, 1978), Vol. 1, p. 868.
[3] S. Krause, in *NATO Advanced Study Institutes Series* (Plenum, New York, 1981), Vol. B64, p. 520.
[4] E. Charney, Q. Rev. Biophys. **21**, 1 (1988).
[5] A. Saupe and W. Maier, Z. Naturforsch. **16**, 816 (1961).
[6] K. Yamaoka and K. Fukudome, J. Phys. Chem. **92**, 4994 (1988).
[7] C. T. O'Konski and A. J. Haltner, J. Am. Chem. Soc. **78**, 3604 (1956).
[8] C. T. O'Konski and A. J. Haltner, J. Am. Chem. Soc. **79**, 5634 (1957).
[9] E. F. Rossomando and J. B. Milstien, J. Mol. Biol. **58**, 187 (1971).
[10] N. Ookubo, Rev. Sci. Instrum. **62**, 948 (1991).
[11] R. Usha and T. A. PrasadaRao, Rev. Sci. Instrum. **65**, 3282 (1994).
[12] H. Asai and N. Watanabe, Biopolymers **15**, 383 (1976).
[13] J. C. Bernengo, B. Roux, and M. Hanss, Rev. Sci. Instrum. **44**, 1083 (1973).
[14] J. Montanha Neto, E. Munin, and A. Balbin Villaverde, Meas. Sci. Technol. **2**, 1026 (1991).
[15] Matlab is available from the MathWorks, Inc. at http://www.mathworks.com
[16] Schematics available upon request.
[17] M. R. Hansen, L. Mueller, and A. Pardi, Nat. Struct. Biol. **5**, 1065 (1998).
[18] http://www.advancedpower.com
[19] Pf1 birefringence is the same sign as that for tobacco mosaic virus, which is known to align with its long axis parallel to *E*. See, for example, M. A. Lauffer, J. Am. Chem. Soc. **61**, 2412 (1939) or C. T. O'Konski and B. H. Zimm, Science **111**, 113 (1950).
[20] J. Torbet and G. Maret, Biopolymers **20**, 2657 (1981).